Valence transition and low field magnetoresistance in $(Sr_{2-x}Ba_x)FeMoO_6$

2004 J. Phys.: Condens. Matter 16 1813

(http://iopscience.iop.org/0953-8984/16/10/013)

INSTITUTE OF PHYSICS PUBLISHING JOURNAL OF PHYSICS: CONDENSED MATTER

J. Phys.: Condens. Matter **16** (2004) 1813–1821 PII: S0953-8984(04)70881-4

Valence transition and low field magnetoresistance in $(Sr_{2-x}Ba_x)FeMoO_6$

X M Feng, G H Rao, G Y Liu, W F Liu, Z W Ouyang and J K Liang

Institute of Physics and Centre for Condensed Matter Physics, Chinese Academy of Sciences, Beijing 100080, People's Republic of China

E-mail: ghrao@aphy.iphy.ac.cn

Received 21 October 2003, in final form 9 February 2004
Published 27 February 2004
Online at stacks.iop.org/JPhysCM/16/1813 (DOI: 10.1088/0953-8984/16/10/013)

Abstract

The crystal structure, electronic transport and magnetic properties of double perovskite $(Sr_{2-x}Ba_x)FeMoO_6$ ($0 \leqslant x \leqslant 2$) are investigated. These compounds exhibit a metal–insulator transition as a function of doping x. The valence transition from Fe^{3+}–Mo^{5+} to Fe^{2+}–Mo^{6+} when x exceeds the critical concentration $x = 1.6$ can lead to a localization of the itinerant electrons and plays a key role in the metal–insulator transition. The bond distance data and composition dependence of the Curie temperature and magnetoresistance suggest this valence transition. The Curie temperature T_C shows an enhancement on the Ba-poor side and decreases monotonically with x on the Ba-rich side, which can be understood in terms of two competing effects: anti-site defects and chemical pressure. The low field magnetoresistance shows a close correlation with the Curie temperature of the compounds.

1. Introduction

Recently, double perovskite oxides $AA'FeMoO_6$ (A, A′ = Sr, Ba) have attracted considerable attention since large low field magnetoresistance (LFMR) was observed in these materials at room temperature. The double perovskite compounds Sr_2FeMoO_6 [1] and Ba_2FeMoO_6 [2] are known to be metallic and ferromagnetic with high magnetic transition temperatures $T_C \sim 400$ and 330 K, respectively. The magnetic structure of Sr_2FeMoO_6 and Ba_2FeMoO_6 was described as an ordered arrangement of parallel Fe^{3+} ($3d^5$, $S = 5/2$) magnetic moments, antiferromagnetically coupled with Mo^{5+} ($4d^1$, $S = 1/2$) spins, and the magnetoresistance (MR) was interpreted as due to intergrain tunnelling of charge carriers because of the half-metallic electronic structure of the compounds [1, 3]. Theoretical electronic structure calculation predicted that the Sr_2FeMoO_6 is a half-metal, where the Mo t_{2g} down-spin band (hybridized with the Fe t_{2g} down-spin band) crosses the Fermi level, but the up-spin band is separated by an insulating gap. The electronic structure of Ba_2FeMoO_6 also reveals that the

states close to the Fermi level E_F are predominantly of Mo $t_{2g}\downarrow$ and Fe $t_{2g}\downarrow$ character [4]. However, the valence states of Fe and Mo ions in the compounds are still in dispute. Neutron diffraction studies support a Fe^{2+} electronic configuration [5, 6], while analysis of Mössbauer and x-ray absorption results suggest the existence of both $Fe^{3-\alpha}$ and Fe^{3+} states [7–10]. Such a disagreement is generally explained by the itinerant t_{2g} electrons of Mo, which can hop through the oxygen orbital to the t_{2g} Fe down-spin empty states, giving no localized moment on the Mo site [5]. Later on, the valence-band PES spectra revealed the mixed-valence Fe^{3+}–Fe^{2+} configurations in Ba_2FeMoO_6 (BFMO) and Sr_2FeMoO_6 (SFMO) compounds and a larger Fe^{2+} component in BFMO than in SFMO [11]. Neutron powder diffraction, Mössbauer spectroscopy and x-ray absorption studies support this result [12]. All methods consistently demonstrate that in Ba_2FeMoO_6 the major interactions are of the Fe^{2+}–O–Mo^{6+} type while in Sr_2FeMoO_6 the major interactions correspond to Fe^{3+}–O–Mo^{5+}. The size of the A-site cation affects the crystalline structure as well as the electronic structure [6, 12]. A close correlation was found between Curie temperature and the electronic bandwidth, which is controlled by structure parameters, of the compounds $AA'FeMoO_6$ ($AA' = Ba_2$, BaSr, Sr_2 and Ca_2) [6].

In this paper, we report a comprehensive study on the structural, electronic and magnetic properties of $(Sr_{2-x}Ba_x)FeMoO_6$ with x ranging from $x = 0$ to 2 to reveal the composition-controlled evolution from itinerant to localized behaviour of the minority-spin electrons. We find that the changes in the electronic transport properties and magnetoresistance are correlated with the changes in the Fe and Mo valences.

2. Experiment

Polycrystalline $(Sr_{2-x}Ba_x)FeMoO_6$ ($0 \leqslant x \leqslant 2$) were prepared by solid-state reaction at high temperature. Stoichiometric amounts of $SrCO_3$, $BaCO_3$, Fe_2O_3 and MoO_3 were mixed and calcined in air at 900 °C for 10 h. The resulting powders were finely pulverized and pressed into pellets followed by sintering at 1280 °C for 3 h in a stream of 5% H_2/Ar with intermediate grindings. X-ray powder diffraction (XRD) patterns of the samples were collected using a Philips X'Pert PRO MPD Alpha-1 system with Cu Kα radiation (45 kV × 40 mA) at room temperature. The field dependence of magnetization was measured at 5 K by a superconducting quantum interference device (SQUID) magnetometer. The temperature dependence of the magnetization curves was measured by a vibrating sample magnetometer (VSM) in a field of 0.05 T. The Curie temperature was determined from the inflection point of the M–T curve. The MR in a field up to 5 T was measured at room temperature with the conventional four-probe method using an OXFORD MaglabExa measurement system.

3. Results and discussion

3.1. Structure

All samples were single-phase and exhibited a series of superstructure reflections due to the ordering of Fe and Mo atoms on the octahedral B sites of a perovskite structure (figure 1). We have refined the structures of $(Sr_{2-x}Ba_x)FeMoO_6$ ($0 \leqslant x \leqslant 2$) based on powder XRD data using the Rietveld program FULLPROF [13]. As reported previously [14], the XRD patterns of all these compositions can be indexed in the space group $Fm3m$ lattice with $Z = 4$, except for that of Sr_2FeMoO_6, which had to be indexed in space group $I4/mmm$ with $Z = 2$. The calculated profile gives a good fit to the observed one as shown in figure 2 ($R_P = 11.3$–15.4%, $R_{WP} = 8.44$–12%, $S = 1.28$–1.6). The lattice parameter increases monotonically with increasing Ba content (figure 3), which is due to the chemical substitution of the larger Ba^{2+}

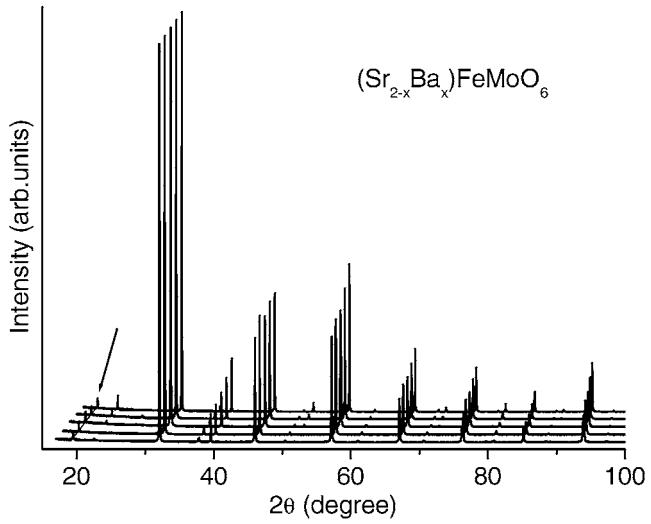

Figure 1. XRD patterns at room temperature for $(Sr_{2-x}Ba_x)FeMoO_6$ ($0 \leqslant x \leqslant 2$) samples. From bottom to top, $x = 0$, 0.5, 1.0, 1.5 and 2, respectively. The arrow indicates the superstructure reflection.

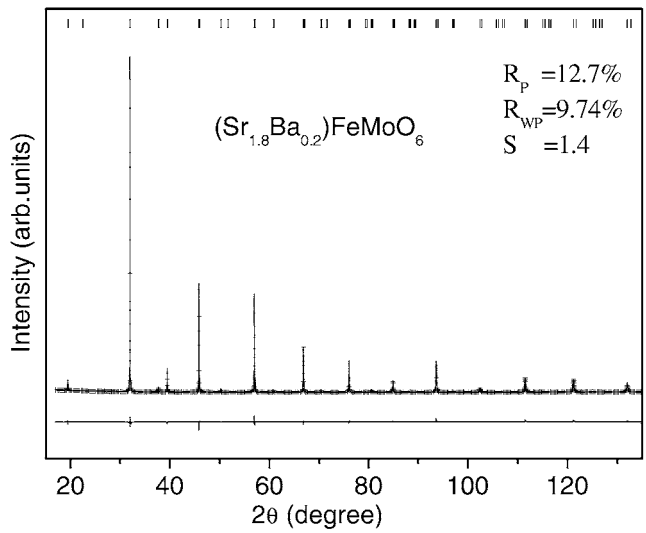

Figure 2. Rietveld refinement of powder XRD data at 300 K for $(Sr_{1.8}Ba_{0.2})FeMoO_6$. Calculated (full curve), experimental (+) and difference (bottom) profiles are shown. The vertical bars at the top indicate Bragg reflection positions.

ions (1.61 Å) for the smaller Sr^{2+} ions (1.44 Å) [15]. The values of the cell parameters are in close agreement with those reported in [14], in which the data for $x = 0.5$, 0.6, 0.84 and 1.42 were given. Refinement of occupancies on the Fe and Mo sites indicates that the anti-site defect decreases with increasing x in the Ba-poor compounds and remains a very small value in Ba-rich compounds (shown in the inset of figure 6). This means an almost perfect ordering of Fe and Mo on the Ba-rich side. The bond length as a function of x in this system is shown in figure 4.

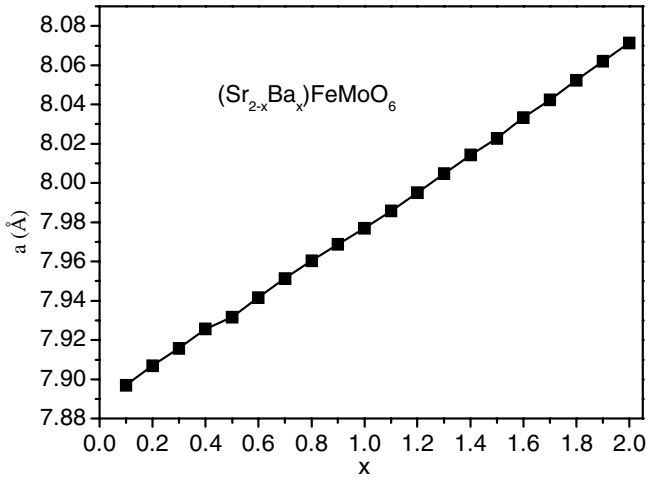

Figure 3. Dependence of the lattice parameter on the doping level x in $(Sr_{2-x}Ba_x)FeMoO_6$ $(0 < x \leqslant 2)$.

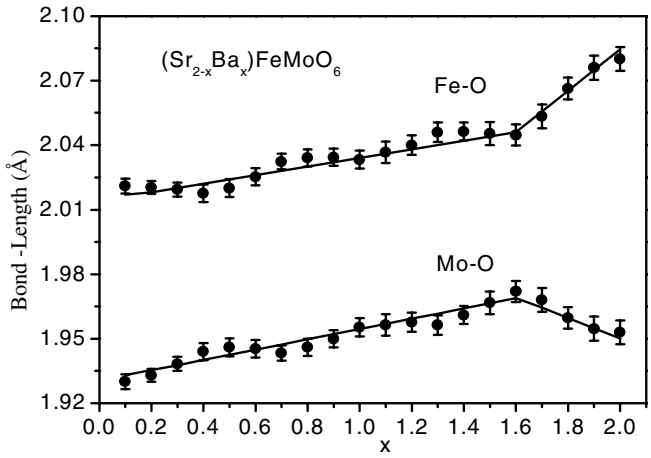

Figure 4. The bond length as a function of x in $(Sr_{2-x}Ba_x)FeMoO_6$ $(0 < x \leqslant 2)$.

3.2. Transport properties

The electrical resistivities (ρ) of all the samples are shown in figure 5 on a logarithmic scale as functions of temperature (T). Evidently, ρ versus T clearly demarcates two regimes. The compounds with $x \leqslant 1.6$ have low resistivities and exhibit metallic behaviour, while the compounds with $x \geqslant 1.7$ are insulating. One of the possible scenarios to explain these observed results is the valence transition from Fe^{3+}–Mo^{5+} to Fe^{2+}–Mo^{6+} in $(Sr_{2-x}Ba_x)FeMoO_6$ by the substitution of Ba for Sr, that is, iron is mostly in the high spin ($S = 5/2$) Fe^{3+} state in Sr_2FeMoO_6, while in Ba_2FeMoO_6 it is closer to the high spin Fe^{2+} ($S = 2$). Band-structure calculations suggest that the ground state of Sr_2FeMoO_6 and Ba_2FeMoO_6 are ferromagnetic metals. The majority spin band structure is insulating, the Fe 3d states are fully occupied and the Mo 4d states are empty, leading to a $S = 5/2$ ferromagnetic moment on each Fe site. The minority spin band is metallic and the occupied part of the band is composed mainly of

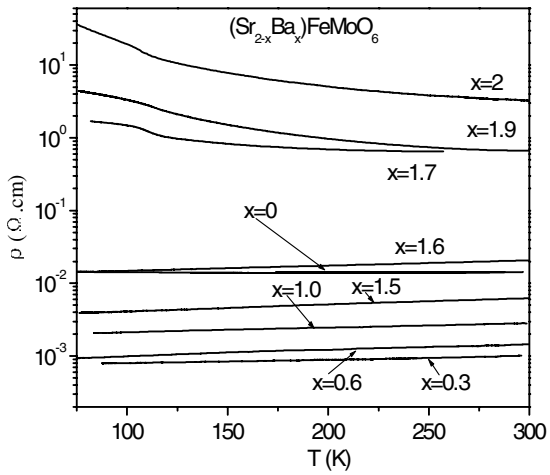

Figure 5. The electrical resistivity of $(Sr_{2-x}Ba_x)FeMoO_6$ as a function of temperature, plotted on a logarithmic scale.

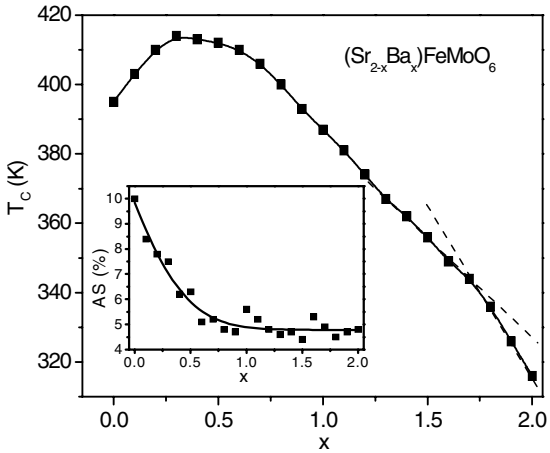

Figure 6. Composition dependence of the Curie temperature T_C of $(Sr_{2-x}Ba_x)FeMoO_6$ ($0 \leqslant x \leqslant 2$). Broken lines are guides to the eyes. Inset: the composition dependence of the anti-site concentration of the compounds.

Mo d states of t_{2g} symmetry. It is shown that an application of pressure or chemical pressure could modify the energy difference between Fe and Mo ($E_{Mo} - E_{Fe}$), which increases with the decrease of pressure or the increase of lattice parameter, and drives the system to the insulating state [16]. In addition, metallic or semiconducting behaviour is very sensitive to sample preparation. In the extreme situation with no carriers on the Mo ions (Fe^{2+} and Mo^{6+}), no states are contributed from the Mo 4d states at the Fermi level E_F, and one could expect that the system is insulating because of the stronger intra-atomic Coulomb repulsion in Fe, compared with the effective Mo–Fe hopping [16]. In our samples, if the valence of Fe^{2+}–Mo^{6+} predominates when x exceeds a critical point, the d state in Mo is not occupied by electrons, which prevents the carriers from being conductive. This suggests that Ba doping in Sr_2FeMoO_6 removes a significant density of states at the Fermi energy, making an insulating state easier to form. This change of transport behaviour is consistent with the notion that in Ba_2FeMoO_6 the

major interactions are of the Fe^{2+}–O–Mo^{6+} type while in Sr_2FeMoO_6 the major interactions correspond to Fe^{3+}–O–Mo^{5+} [11, 12]. The tendency of the valence transition from Fe^{3+}–Mo^{5+} to Fe^{2+}–Mo^{6+} is strongly supported by the bond distance data shown in figure 4. When x exceeds 1.6, the Fe–O bond length increased steeply and the Mo–O bond length decreased in the same way. Because the radii of Fe^{2+} are larger than that of Fe^{3+} and the radii of Mo^{6+} are smaller than that of Mo^{5+}, it is reasonable to expect that the abrupt change in bond distance is due to the valence transition.

3.3. Magnetic properties

The Curie temperature T_C as a function of the doping content x is shown in figure 6. T_C increases to a maximum value at $x = 0.4$ and then decreases until $x = 2$. The T_C values are in very good agreement with those reported by Galasso *et al* [14], except for Sr_2FeMoO_6 and Ba_2FeMoO_6, the Curie temperatures of which are slightly lower than those reported ($T_C = 334$ and 422 K for $AA' = Ba_2$ and Sr_2, respectively), but higher than those reported in [6] ($T_C = 308$, 340 and 385 K for $AA' = Ba_2$, BaSr, and Sr_2, respectively). The difference in T_C can arise from the synthesis methods used by different authors, which may modify the cationic ordering and the oxygen and cationic stoichiometry. The composition dependence of T_C can be understood in terms of two competing factors: the anti-site defects and chemical pressure. The presence of Fe/Mo anti-site defects destroys the half-metallic ferromagnetic state, which is detrimental to the double-exchange-like interaction and would lead to a decrease of T_C [17, 18]. On the other hand, as the amount of Ba increases, the A-site average ionic radius $\langle r_A \rangle$ increases within the cubic symmetry, which can result in a narrower bandwidth (W) and thus reduce the T_C, as argued in [6, 14]. At small Ba doping, the anti-site defect decreases with Ba doping and the effect of anti-site defects exceeds the effect of the chemical pressure. Therefore, in our samples the T_C exhibits an enhancement up to $x = 0.4$. As the Ba content increases, an almost perfect ordering of Fe and Mo indicates that the B-site disorder is not important for the magnetic interaction and electronic transport in these compounds and thus the effect of the $\langle r_A \rangle$ on the T_C becomes dominant. As x increases, the $\langle r_A \rangle$ increases and the electronic bandwidth decreases, leading to the decrease of T_C. As shown in figure 6, there is a noticeable inflection around $x = 1.7$. When the doped content exceed $x = 1.6$, the T_C decreases at a different slope and more steeply. The less itinerant conduction electron is amenable to this phenomenon, which also supports the tendency of the valence transition from Fe^{3+}–Mo^{5+} to Fe^{2+}–Mo^{6+} when x exceeds the critical concentration.

The magnetization isotherm measured at 5 K is typically ferromagnetic with negligible remanence and coercivity, as illustrated in figure 7. The rapid rise of the low field magnetization of the Ba-doped samples, compared with that of the Sr_2FeMoO_6, indicates that the Ba-doped samples are magnetically softer, which is consistent with the reports in [19] and [20], where the substitution of Ba for Sr tends to decrease both the remanent magnetization and coercivity H_C. Figure 8 shows the composition dependence of the saturation magnetization M_S at 5 K. M_S are derived by extrapolating $1/H$ to zero on the M–$1/H$ curve. The rapid increase of M_S in the low-x region, coincident with the trend of T_C, could be explained by the effect of anti-site defects, which clearly decreases with x in this regime, as shown in the inset of figure 6. All values are lower than the ideal 4 μ_B/fu and could be attributed to the effect of anti-site defects and other effects, such as the presence of oxygen vacancies or off-stoichiometries [17, 21].

Figure 9 displays the behaviour of the MR versus the external applied field at room temperature for $x = 0$, 0.4 and 1.6. The MR is defined as $\mathrm{MR}(H, T) = \{\rho(H, T) - \rho(0, T)\}/\rho(0, T)$. The |MR| increases much more rapidly in the low field region than in the high field regime. Here, we focus our attention on the low field region,

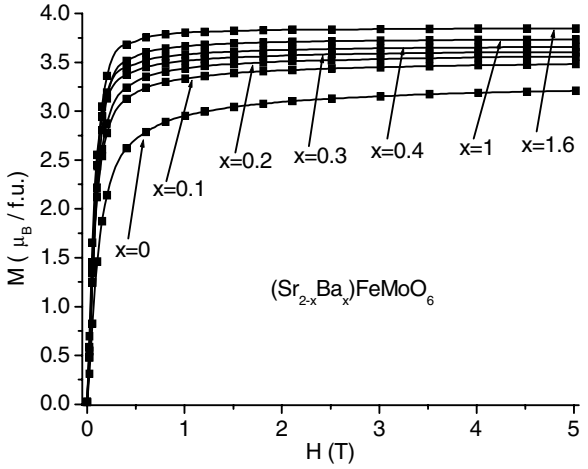

Figure 7. Typical magnetization isotherms of $(Sr_{2-x}Ba_x)FeMoO_6$ at 5 K.

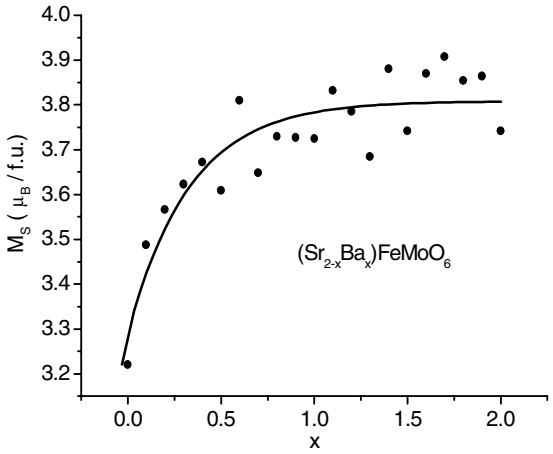

Figure 8. The variation of the saturation magnetization of $(Sr_{2-x}Ba_x)FeMoO_6$ with x at 5 K. The curve is a guide for the eyes.

which is most interesting for practical applications of the materials. Figure 10 shows the behaviour of the percentage of variation of the LFMR per unit applied field (approximately defined as $\{MR(0) - MR(0.1\ T)\}/0.1\ T$) as a function of the Ba content x at room temperature. $\rho(H)/\rho(0)$ versus applied magnetic field ($-0.5\ T \leqslant H \leqslant 0.5\ T$) for a set of representative samples is shown in the inset of figure 10. Roughly, the LFMR is enhanced substantially as x increases for $x \leqslant 0.4$, decreases gradually for $0.4 < x \leqslant 1.6$ and drops to a very small value for $x \geqslant 1.7$. The irregularities at $x = 0.5$, 0.6, 0.7 and 1.0 may be due to the quality of the samples. In [19], the optimization of the LFMR was found at $(Sr_{0.4}Ba_{1.6})FeMoO_6$ and the author attributed this to the soft magnetic behaviour. Among our Ba-doped samples, the degree of magnetic softness is approximately the same, while a close correlation between T_C and LFMR seems plausible. When the doping content exceeds the critical value $x = 1.6$, an increasing population of localized-electron Fe^{2+} configurations would reduce the itinerant electrons and weaken the double-exchange interaction, leading to a much smaller LFMR.

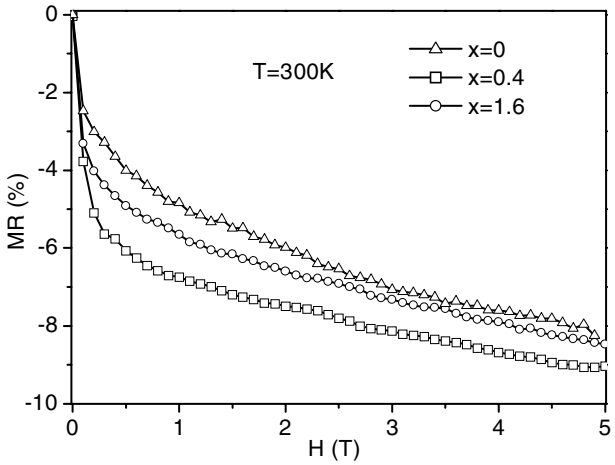

Figure 9. Room temperature magnetoresistance of $(Sr_{2-x}Ba_x)FeMoO_6$ ($x = 0$, 0.4 and 1.6) versus applied field H.

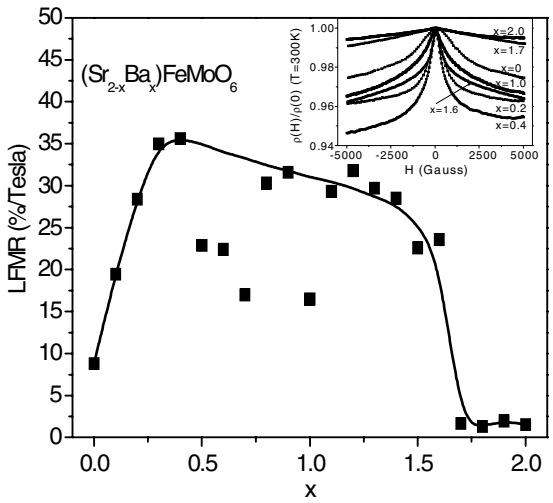

Figure 10. LFMR per unit of applied field versus doped content x in $(Sr_{2-x}Ba_x)FeMoO_6$ ($0 \leqslant x \leqslant 2$). Inset: $\rho(H)/\rho(0)$ versus applied magnetic field for a set of representative samples.

4. Conclusion

In conclusion, the crystal structure, magnetization and magnetoresistance of $(Sr_{2-x}Ba_x)FeMoO_6$ ($0 \leqslant x \leqslant 2$) are investigated. The resistivity and magnetoresistance measurements clearly distinguish two composition regimes. In the first regime, with $x \leqslant 1.6$, the compounds have low resistivities and exhibit metallic behaviour, while in the second regime, with $x \geqslant 1.7$, the compounds are insulating. The valence transition plays a key role in the metal–insulator transition as a function of x for the compounds investigated. The valence transition of Fe from 3+ to the 2+ state can lead to the localization of the itinerant electrons and an insulating behaviour of the compounds. The Curie temperature T_C shows an enhancement on the Ba-poor side and decreases monotonically with x on the Ba-rich side, which can be understood by two

competing effects: anti-site defects and chemical pressure. The low field magnetoresistance seems to show a close correlation with the Curie temperature of the compounds.

Acknowledgments

This work is supported by the National Natural Foundation of China and by State Key Project of Fundamental Research.

References

[1] Kobayashi K-I, Kimura T, Sawada H, Terakura K and Tokura Y 1998 *Nature* **395** 677
[2] Maignan A, Raveau B, Martin C and Hervieu M 1999 *J. Solid State Chem.* **144** 224
[3] Sleight A W and Weiher J F 1972 *J. Phys. Chem. Solids* **33** 679
[4] Kang J S, Han H, Lee B W, Olson C G, Han S W, Kim K H, Jeong J I, Park J H and Min B I 2001 *Phys. Rev.* B **64** 024429
[5] García-Landa B, Ritter C, Ibarra M R, Blasco J, Algarabel P A, Mahendiran R and García J 1999 *Solid State Commun.* **110** 435
[6] Ritter C, Ibarra M R, Morellon L, Blasco J, Garcia J and De Teresa J M 2000 *J. Phys.: Condens. Matter* **12** 8295
[7] Lindén J, Yamamono T, Karppinen M and Yamauchi H 2000 *Appl. Phys. Lett.* **76** 2925
[8] Greneche J M, Venkatesan M, Suryanarayanan R and Coey J M D 2001 *Phys. Rev.* B **63** 174403
[9] Ray S, Kumar A, Sarma D D, Cimino R, Turchini S, Zennaro S and Zema N 2001 *Phys. Rev. Lett.* **87** 097204
[10] Sarma D D, Sampathkumaran E V, Ray S, Nagarajan R, Majumdar S, Kumar A, Nalini G and Row T N G 2000 *Solid State Commun.* **114** 465
[11] Kang J-S, Kim J H, Sekiyama A, Kasai S, Suga S, Han S W, Kim K H, Muro T, Saitoh Y, Hwang C, Olson C G, Park B J, Lee B W, Shim J H, Park J H and Min B I 2002 *Phys. Rev.* B **66** 113105
[12] Nguyen N, Sriti F, Martin C, Bourée F, Grenèche J M, Ducouret A, Studer F and Raveau B 2002 *J. Phys.: Condens. Matter* **14** 12629
[13] Rodriguez-Carvajal J 1998 *FULLPROF, Version 3.1d-LLB-JRC* (France: ILL)
[14] Galasso F S, Douglas F C and Kasper R J 1966 *J. Chem. Phys.* **44** 1672
[15] Shannon R D 1976 *Acta Crystallogr.* A **32** 751
[16] Aligia A A, Petrone P, Sofo J O and Alascio B 2001 *Phys. Rev.* B **64** 092414
[17] Ogale A S, Ogale S B, Ramesh R and Venkatesan T 1999 *Appl. Phys. Lett.* **75** 537
[18] Saha-Dasgupta T and Sarma D D 2001 *Phys. Rev.* B **64** 064408
[19] Kim B-G, Hor Y-S and Cheong S-W 2001 *Appl. Phys. Lett.* **79** 388
[20] Zhou J P, Dass R, Yin H Q, Zhou J-S, Rabenberg L and Goodenough J B 2000 *J. Appl. Phys.* **87** 5037
[21] Balcells L I, Navarro J, Bibes M, Roig A, Martínez B and Fontcuberta J 2001 *Appl. Phys. Lett.* **78** 781